Magnetic to magnetic and kinetic to magnetic energy transfers at the top of the Earth's core

Ludovic Huguet,[1,2] Hagay Amit[3] and Thierry Alboussière[2]

[1]*Department of Earth, Environmental, and Planetary Sciences, Case Western Reserve University, Cleveland, OH* 44106, *USA.*
E-mail: *ludovic.huguet@case.edu*
[2]*CNRS UMR* 5276, *Université Lyon* 1, *ENS Lyon, Laboratoire de Géologie de Lyon, Terre, Planètes, Environnement,* 2 *rue Raphaël Dubois, Villeurbanne F-*69622, *France*
[3]*CNRS UMR* 6112, *Université de Nantes, Laboratoire de Planétologie et de Géodynamique,* 2 *rue de la Houssinière, Nantes F-*44000, *France*

SUMMARY
We develop the theory for the magnetic to magnetic and kinetic to magnetic energy transfer between different spherical harmonic degrees due to the interaction of fluid flow and radial magnetic field at the top of the Earth's core. We show that non-zero secular variation of the total magnetic energy could be significant and may provide evidence for the existence of stretching secular variation, which suggests the existence of radial motions at the top of the Earth's core—whole core convection or MAC waves. However, the uncertainties of the small scales of the geomagnetic field prevent a definite conclusion. Combining core field and flow models we calculate the detailed magnetic to magnetic and kinetic to magnetic energy transfer matrices. The magnetic to magnetic energy transfer shows a complex behaviour with local and non-local transfers. The spectra of magnetic to magnetic energy transfers show clear maxima and minima, suggesting an energy cascade. The kinetic to magnetic energy transfers, which are much weaker due to the weak poloidal flow, are either local or non-local between degree one and higher degrees. The patterns observed in the matrices resemble energy transfer patterns that are typically found in 3-D MHD numerical simulations.

Key words: Dynamo: theories and simulations; Geomagnetic induction; Magnetic field; Rapid time variations; Core, outer core and inner core.

1 INTRODUCTION

The geomagnetic field is generated by convection-driven flow of an electrically conducting fluid at Earth's outer core. This dynamo process is maintained by the transfer of kinetic energy to magnetic energy (Moffatt 1978). Inferring energy transfers at the top of the Earth's core may provide vital information about the geodynamo. Here we focus on two possible applications, (i) dipole changes and (ii) the existence of a stable layer. Models of the geomagnetic field and its secular variation (SV) based on surface observatories and recent satellite data (Jackson *et al.* 2000; Olsen & Mandea 2008; Olsen *et al.* 2014) show that the radial field at the core–mantle boundary (CMB) is dominated by an axial dipole component. Since the advent of geomagnetic measurements about 170 yr ago, the geomagnetic dipole intensity has been rapidly decreasing (Olson & Amit 2006; Finlay 2008). Recent experimental and numerical mineral physics (Pozzo *et al.* 2012; Vlček *et al.* 2012; Gomi *et al.* 2013) and seismic (Helffrich & Kaneshima 2010) studies suggest that the top of core is stably stratified (Gubbins & Davies 2013).

Studies on changes in the dipole focused mostly on a spatial approach (Gubbins 1987; Olson & Amit 2006). For example, Gubbins (1987) used the integral form of the axial dipole to argue

that the growth of reversed flux patches is responsible for the historical decrease in the dipole intensity. Finlay *et al.* (2012) found that the spatial contributions to axial dipole change are governed by small scales with a large amount of cancellations. Many numerical dynamos studies showed that reversed flux patches on the CMB trigger dipole collapse (Wicht & Olson 2004; Takahashi *et al.* 2007; Aubert *et al.* 2008; Olson *et al.* 2009). Alternatively, dipole changes can be studied via a spectral approach (Amit & Olson 2010; Huguet & Amit 2012). In analogy with classical turbulence theory for an homogeneous isotropic medium (Kolmogorov 1941; Batchelor 1953; Frisch 1995), Amit & Olson (2010) found that forward energy cascade within the equatorially anti-symmetric field may explain the dipole decrease. Huguet & Amit (2012) extended the spectral approach, permitting both local and non-local transfers. Combining core field and flow models, they associated the dipole decrease to both forward energy cascade and non-local transfer from the dipole directly to high degrees.

Stable stratification at the top of the core was proposed based on relatively low geomagnetic SV at extreme points where advection vanishes (Whaler 1980). In contrast, later studies argued that poloidal flow is needed to explain the SV (Whaler 1986) and that relying on specific grid points is uncertain (Whaler & Holme

2007). It was even demonstrated (somewhat provocatively) that a pure poloidal flow could explain the SV, although such a flow is not thought to be realistic (Beggan & Whaler 2008). Lesur *et al.* (2015) inverted geomagnetic data simultaneously for the field and the core flow. They could not adequately fit the data with a purely toroidal flow, but inclusion of a weak poloidal flow was sufficient. Lesur *et al.* (2015) concluded that satellite geomagnetic data are compatible with a weakly stratified layer at the top of the core. Interpretations of SV on regional scale also supported the existence of upwelling (Olson & Aurnou 1999; Chulliat & Olsen 2010) or downwelling (Amit 2014). Global core flow inversions usually assume some relation between toroidal and poloidal flows (for review see Holme 2015). Quasi-geostrophic core flows rely on poloidal flows to project surface flows to the volume of the outer core (Pais & Jault 2008; Gillet *et al.* 2009). Such projections would not hold if the top of the core is stratified. Seismic studies (Helffrich & Kaneshima 2010) found a reduced velocity at the top of the outer core. Large values of thermal and electrical conductivities of iron alloy at core conditions suggest that the core adiabat is very close to the total CMB heat flux (Pozzo *et al.* 2012; Vlček *et al.* 2012; Gomi *et al.* 2013). If that is the case, the geodynamo is maintained by compositional convection at depth, the top of the core is stably stratified, and the flow at the top of the core may be purely toroidal. It should be noted that depending on the associated time and length scales radial flow may penetrate a stably stratified layer, for example, if the convection columns are large enough (Takehiro & Lister 2001), in the presence of waves (Buffett 2014) or at quasi-geostrophic conditions (Vidal & Schaeffer 2015). In contrast, it was recently argued that the thermal conductivity is as low as the early estimates and therefore the whole of the core convects (Konôpková *et al.* 2016; Ohta *et al.* 2016). The existence of stably stratified layer in general means that there is zero stretching at the top of the core, that is, zero kinetic to magnetic energy transfer (Alexakis *et al.* 2005a). An exception is the scenario of vertical velocities in the stratified layer that can be provided by MAC waves (Buffett 2014; Buffett *et al.* 2016), which arise from the dominance of the magnetic, Archimedes and Coriolis forces. The MAC waves can explain the presence of the 60-yr fluctuations observed in the Earth's magnetic field (Currie 1973; Roberts *et al.* 2007; Jackson & Mound 2010) and part of the observed fluctuations in the length of day (Gross 2001; Holme & De Viron 2013) with the remaining signal possibly attributed to deeper motions.

In a preliminary study, Huguet & Amit (2012) combined core field and flow models to calculate the magnetic to magnetic power transfer. Based on the shape of the degree-dependent integrated transfer spectra, they divided the historical period to three subintervals. They found that the geomagnetic power transfer is very complex with a local Kolmogorov-like transfer and non-local transfer. The transfer power spectrum reverses even maxima and odd minima for the period 1840–1910 to odd maxima and even minima for the period 1955–1990.

The formalism derived in this paper differs from that of Huguet & Amit (2012) in two important ingredients. First, motivated by geomagnetic convention, Huguet & Amit (2012) calculated power transfers. Here we compute energy transfers, which are more justified physically. In addition, energy transfer has some elegant theoretical properties: The total magnetic to magnetic energy transfer is identically zero, and the magnetic to magnetic energy transfer matrix is anti-symmetric about the main diagonal (Alexakis *et al.* 2005a,b, 2007; Mininni 2011). Second, Huguet & Amit (2012) attributed the SV of the magnetic energy entirely to magnetic to magnetic transfer. Here we perform a complete analysis

including both magnetic to magnetic and kinetic to magnetic energy transfers.

The paper is outlined as follows. In Section 2, we introduce a formalism to calculate the magnetic to magnetic and kinetic to magnetic energy transfers that account for the SV in the total geomagnetic energy in 3-D with full magnetic field vector and in 2-D with radial magnetic field only. The SV of the total geomagnetic energy based on the field and SV from historical (Jackson *et al.* 2000; Gillet *et al.* 2013) and satellites (Olsen *et al.* 2014) observations are presented in the first part of Section 4. Combining core field and flow models, magnetic to magnetic and kinetic to magnetic energy transfers are examined in the second part of Section 4. We discuss our main results in Section 5.

2 THEORY

The total magnetic energy is generally defined as the volume integral of the intensity of the magnetic field vector. However, a similar definition may be applied for the radial component of the field on the CMB surface. In the frozen-flux limit where magnetic diffusion is neglected, the SV of the magnetic energy is due to magnetic to magnetic energy transfer and kinetic to magnetic energy transfer. Below we compare the expressions for the two energy transfers in a 3-D spherical shell volume and in a 2-D spherical surface with only a radial magnetic field component, the latter applicable to the available information in geomagnetism. We then derive corresponding expressions for the energy transfer spectra and relate them to the SV of the geomagnetic power spectrum.

2.1 Energy transfer in 3-D with full magnetic field vector

The 3-D magnetic induction equation in the frozen-flux limit is

$$\frac{\partial \overrightarrow{B}}{\partial t} = -(\overrightarrow{u} \cdot \nabla)\overrightarrow{B} + (\overrightarrow{B} \cdot \nabla)\overrightarrow{u}, \tag{1}$$

where $\overrightarrow{B}$ is the magnetic field vector, $\overrightarrow{u}$ is the velocity vector and t is time. The second and last terms in eq. (1) are the contributions to SV by magnetic field advection and stretching, respectively. Multiplying eq. (1) by $\overrightarrow{B}/\mu_0$ gives

$$\frac{1}{2\mu_0}\frac{\partial B^2}{\partial t} = -\frac{1}{2\mu_0}(\overrightarrow{u}\cdot\nabla)B^2 + \frac{1}{\mu_0}\overrightarrow{B}\cdot((\overrightarrow{B}\cdot\nabla)\overrightarrow{u}), \tag{2}$$

where B^2 represents the squared field intensity and μ_0 is the permeability of free space. The first term in eq. (2) is the integrand of the SV of the total magnetic energy:

$$\dot{E}_b = \int_V \frac{1}{2\mu_0}\frac{\partial B^2}{\partial t}dV, \tag{3}$$

where V is the volume of the spherical shell.

We define the magnetic to magnetic energy transfer $\dot{e}_{bb}$ and the kinetic to magnetic energy transfer $\dot{e}_{ub}$ (Alexakis *et al.* 2005b; Debliquy *et al.* 2005; Mininni *et al.* 2005; Lessinnes *et al.* 2009) so that (i) their sum corresponds to the total magnetic energy change (right-hand side of eq. 2), (ii) the integral of $\dot{e}_{bb}$ over the physical space is obviously zero, for any possible velocity and magnetic fields, (iii) the contribution $\dot{e}_{ub}$ may obviously have an integrated non-zero contribution for a certain velocity and magnetic field. Integrating the advection term gives

$$\int_V (\overrightarrow{u}\cdot\nabla)\frac{B^2}{2\mu_0}dV = \int_V \nabla\cdot\left(\overrightarrow{u}\frac{B^2}{2\mu_0}\right)dV - \int_V \frac{B^2}{2\mu_0}(\nabla\cdot\overrightarrow{u})dV. \tag{4}$$

The last term in eq. (4) vanishes due to conservation of mass in incompressible conditions ($\nabla \cdot \overrightarrow{u} = 0$). Applying the divergence theorem for the second term in eq. (4) gives

$$\int \nabla \cdot \left(\overrightarrow{u} \frac{B^2}{2\mu_0} \right) dV = \int_S \overrightarrow{u} \frac{B^2}{2\mu_0} \hat{r} dS = \int_S u_r \frac{B^2}{2\mu_0} dS = 0, \quad (5)$$

where S is the surface of the outer boundary of the shell. Because $u_r = 0$ on the rigid CMB, we therefore find that the magnetic to magnetic energy transfer is due to the advection term,

$$\dot{e}_{bb} = -\frac{1}{2\mu_0} (\overrightarrow{u} \cdot \nabla) B^2 \quad (6)$$

and the kinetic to magnetic energy transfer is due to the stretching term,

$$\dot{e}_{ub} = \frac{1}{\mu_0} \overrightarrow{B} \cdot ((\overrightarrow{B} \cdot \nabla) \overrightarrow{u}) \quad (7)$$

where $\dot{e}_{bb}$ and $\dot{e}_{ub}$ in eqs (6) and (7) are functions of longitude, co-latitude and radius, which denote spatial contributions to the SV of the magnetic energy.

2.2 Energy transfer in 2-D with radial magnetic field

The radial magnetic induction equation in the frozen-flux limit on the CMB (where $u_r = 0$) is

$$\frac{\partial B_r}{\partial t} = -\overrightarrow{u_h} \cdot \nabla_h B_r - B_r \nabla_h \cdot \overrightarrow{u_h} \quad (8)$$

Multiplying eq. (8) by B_r/μ_0 gives

$$\frac{1}{2\mu_0} \frac{\partial B_r^2}{\partial t} = -\overrightarrow{u_h} \cdot \nabla_h \frac{B_r^2}{2\mu_0} - \frac{B_r^2}{\mu_0} \nabla_h \cdot \overrightarrow{u_h} \quad (9)$$

The first term in eq. (9) is the integrand of the SV of the total (poloidal) magnetic energy:

$$\dot{E}_b = \frac{1}{4\pi} \int_S \frac{1}{2\mu_0} \frac{\partial B_r^2}{\partial t} dS. \quad (10)$$

The error associated with our discrete numerical integration in eq. (10) is around 0.1 per cent. We note that applying the same identity as in the 3-D case will yield a different result because the tangential divergence that is relevant for the 2-D case is in general non-zero. We therefore split the stretching term in eq. (9) into two halves:

$$\frac{1}{2\mu_0} \frac{\partial B_r^2}{\partial t} = -\overrightarrow{u_h} \cdot \nabla_h \frac{B_r^2}{2\mu_0} - \frac{B_r^2}{2\mu_0} \nabla_h \cdot \overrightarrow{u_h} - \frac{B_r^2}{2\mu_0} \nabla_h \cdot \overrightarrow{u_h}. \quad (11)$$

Combining the second and third terms of eq. (11) gives

$$\frac{1}{2\mu_0} \frac{\partial B_r^2}{\partial t} = -\nabla_h \cdot \left(\overrightarrow{u_h} \frac{B_r^2}{2\mu_0} \right) - \frac{B_r^2}{2\mu_0} \nabla_h \cdot \overrightarrow{u_h}. \quad (12)$$

The divergence theorem (or Green's theorem) for wrapped 2-D surfaces like the spherical CMB gives trivially zero value for the integrals. Therefore, integrating the second term of eq. (12) gives

$$\int_S \nabla_h \cdot \left(\overrightarrow{u_h} \frac{B_r^2}{2\mu_0} \right) dS = 0. \quad (13)$$

We thus obtain for the 2-D case with only radial magnetic field

$$\dot{e}_{bb} = -\overrightarrow{u_h} \cdot \nabla_h \frac{B_r^2}{2\mu_0} - \frac{B_r^2}{2\mu_0} \nabla_h \cdot \overrightarrow{u_h} \quad (14)$$

and

$$\dot{e}_{ub} = -\frac{B_r^2}{2\mu_0} \nabla_h \cdot \overrightarrow{u_h}. \quad (15)$$

Note that here the magnetic to magnetic transfer is due to the advection term plus half the stretching term, and the kinetic to magnetic transfer is due to half the stretching term.

2.3 Energy transfer spectra

The magnetic field power spectrum R_n at the CMB is given by (Lowes 1974)

$$R_n = (n+1) \left(\frac{a}{c} \right)^{2n+4} \sum_{m=0}^{n} \left((g_n^m)^2 + (h_n^m)^2 \right), \quad (16)$$

where a is Earth's radius, c is the radius of the core and g_n^m and h_n^m are the Gauss coefficients of the core field at spherical harmonic degree and order n and m, respectively. The SV of the field power spectrum is written as (Cain *et al.* 1989; Amit & Olson 2010; Huguet & Amit 2012)

$$\dot{R}_n = 2(n+1) \left(\frac{a}{c} \right)^{2n+4} \sum_{m=0}^{n} \left(g_n^m \dot{g}_n^m + h_n^m \dot{h}_n^m \right). \quad (17)$$

In the frozen-flux limit the SV of the magnetic power spectrum can be written as the sum of power transfer spectra

$$\dot{R}_n = T_{bb}^n + T_{ub}^n, \quad (18)$$

where the power transfer spectra T_{bb}^n and T_{ub}^n are functions of spherical harmonic degree. The formalism to obtain these functions is given in details in Section 3.2. The energy is related to the power by a degree-dependent factor (see e.g. eq. 7 of Amit & Olson 2010). The same factor relates the energy transfer spectra and power transfer spectra:

$$\dot{E}_{bb}^n = \frac{1}{2\mu_0} \left(\frac{n+1}{2n+1} \right) T_{bb}^n \quad (19)$$

$$\dot{E}_{ub}^n = \frac{1}{2\mu_0} \left(\frac{n+1}{2n+1} \right) T_{ub}^n, \quad (20)$$

where $\dot{E}_{bb}^n$ and $\dot{E}_{ub}^n$ are also functions of spherical harmonic degree. From the spatial integration of eq. (14), the total magnetic to magnetic energy transfer is identically zero:

$$\sum_{n=1}^{n_{max}} \dot{E}_{bb}^n = -\frac{1}{4\pi} \int_S \nabla_h \cdot \left(\overrightarrow{u_h} \frac{B_r^2}{2\mu_0} \right) dS$$

$$= \sum_{n=1}^{n_{max}} \frac{1}{2\mu_0} \left(\frac{n+1}{2n+1} \right) T_{bb}^n = 0. \quad (21)$$

From the spatial integration of eq. (15), the total kinetic to magnetic energy transfer is written as

$$\sum_{n=1}^{n_{max}} \dot{E}_{ub}^n = -\frac{1}{4\pi} \int_S \frac{B_r^2}{2\mu_0} \nabla_h \cdot \overrightarrow{u_h} dS = \sum_{n=1}^{n_{max}} \frac{1}{2\mu_0} \left(\frac{n+1}{2n+1} \right) T_{ub}^n. \quad (22)$$

By definition the total of kinetic to magnetic energy transfer is equal to the SV of the total magnetic energy $\dot{E}_b$ (10):

$$\dot{E}_b = \sum_{n=1}^{n_{max}} \dot{E}_{ub}^n. \quad (23)$$

3 METHOD

3.1 Measures of the secular variation of the total magnetic energy

To test whether the numerical values that we obtain for the SV of the total magnetic energy are significant, we define ratios of integrals with respect to their corresponding absolute integrals. Such integral ratios quantify the level of spatial cancellations at a given integral and may therefore assess the significance of the numerical values.

The ratio ε_e is defined by

$$\varepsilon_e = \frac{\int_S B_r \frac{\partial B_r}{\partial t} \, \mathrm{d}S}{\int_S |B_r \frac{\partial B_r}{\partial t}| \, \mathrm{d}S}. \tag{24}$$

This ratio represents the SV of the total magnetic energy. For comparison, the ratio ε_{mz} represents the SV of the axial dipole (Moffatt 1978; Davidson 2001; Olson & Amit 2006) and is written as

$$\varepsilon_{mz} = \frac{\int_S \cos\theta \frac{\partial B_r}{\partial t} \, \mathrm{d}S}{\int_S |\cos\theta \frac{\partial B_r}{\partial t}| \, \mathrm{d}S}. \tag{25}$$

Because the geomagnetic field is observed at Earth's surface where no significant spatial cancellations appear, there is certainly no doubt that the dipole is decreasing. The ratio ε_{mz} therefore serves as a reference value to the level of cancellations that cannot be considered negligible.

Finally, the ratio ε_{sv} simply denotes the integrated SV and is written

$$\varepsilon_{sv} = \frac{\int_S \frac{\partial B_r}{\partial t} \, \mathrm{d}S}{\int_S |\frac{\partial B_r}{\partial t}| \, \mathrm{d}S} = 0. \tag{26}$$

The theoretical value of ε_{sv} is identically zero. Based on our calculated ε_{sv} values in the gufm1 model (Jackson *et al.* 2000), the error in our numerical integration is as small as about 0.035 per cent.

3.2 Measures of the energy transfer spectra

For the magnetic to magnetic energy transfer spectrum, we calculate the contribution to the SV of the magnetic energy from advection plus half stretching, based on the eq. (14)

$$\frac{\partial B_r^{bb}}{\partial t} = -\overrightarrow{u_h} \cdot \nabla_h B_r^p - \frac{1}{2} B_r^p \nabla_h \cdot \overrightarrow{u_h}. \tag{27}$$

We calculate the interaction of degree p of the field B_r^p with the full flow $\overrightarrow{u_h}$. We then apply a spectral transform to obtain the SV Gauss coefficients $\dot{g}_n^m$ and $\dot{h}_n^m$, and in conjunction with the field Gauss coefficients g_p^m and h_p^m we compute the power transfer spectrum based on eqs (17) and (18) and convert to magnetic to magnetic energy transfer spectrum using eq. (19). The matrix term at column p and line s, $\dot{E}_{bb}(p, s)$, denotes the magnetic energy transferred from degree p of the field to degree s of the field. Because the matrix $\dot{E}_{bb}(p, s)$ is antisymmetric (e.g. Alexakis *et al.* 2005a, 2007), we fold the lower part into the part above the main diagonal. Negative $\dot{E}_{bb}(p, s)$ represents energy transfer from degree s of the field to degree p of the field.

For kinetic to magnetic energy transfer spectrum, we calculate the contribution to the SV of the magnetic energy from half stretching of the radial field B_r by the flow of degree p $\overrightarrow{u}_h^{\ p}$, based on eq. (15)

$$\frac{\partial B_r^{ub}}{\partial t} = -\frac{1}{2} B_r \nabla_h \cdot \overrightarrow{u_h}^p. \tag{28}$$

We then apply a spectral transform to obtain the SV Gauss coefficients $\dot{g}_n^m$ and $\dot{h}_n^m$, and in conjunction with the field Gauss coefficients g_n^m and h_n^m we compute the kinetic to magnetic power transfer spectrum based on eqs (17) and (18) and convert to kinetic to magnetic energy transfer spectrum using eq. (20). We denote as $\dot{E}_{ub}(p, q)$ the energy transferred from degree p of the flow to degree q of the field due to the interaction of the total magnetic field B_r with degree p of the flow $\overrightarrow{u_h}^p$. Negative $\dot{E}_{ub}(p, q)$ represents energy transfer from degree q of the field to degree p of the flow.

We also calculate the integrated magnetic to magnetic energy transfer for each degree strictly due to transfer within the observed spectrum $n_{\max} \geq n \geq 1$, from hereafter denoted by $\dot{E}_{bb}^s (n_{\max})$, as

$$\dot{E}_{bb}^s(n_{\max}) = \sum_{p=1}^{s-1} \dot{E}_{bb}(p, s) - \sum_{p=s+1}^{n_{\max}} \dot{E}_{bb}(s, p). \tag{29}$$

Similar to eq. (29), we also calculate the integrated spectrum $\dot{E}_{ub}^q(n_{\max})$ as

$$\dot{E}_{ub}^q(n_{\max}) = \sum_{p=1}^{n_{\max}} \dot{E}_{ub}(p, q). \tag{30}$$

Finally, we compute the integrated energy transfers including energy leaking beyond the observed spectrum. We calculate the SV from the interaction of the full field B_r with the full flow, from hereafter denoted by $\dot{E}_{bb} (\infty)$ and $\dot{E}_{ub} (\infty)$. All these integrated energy transfer quantities are compared with the observed integrated power transfer based on the Gauss coefficients of the field and its SV (17) and factored to energy transfer.

All energy spectra and matrices are integrated over all orders m. However, the theory is available to track energy transfers between each pair of spherical harmonics degrees and orders. Here we focus on the order integrated quantities as in previous studies of the geomagnetic field and SV spectra (Lowes 1974; Cain *et al.* 1989; Holme *et al.* 2011; Lhuillier *et al.* 2011; Christensen *et al.* 2012).

4 RESULTS

First we analyse the SV of the total geomagnetic energy based on core field and SV models. In section 4.1, we examine whether the non-zero SV of the total geomagnetic energy is robust using the geomagnetic field and SV models gufm1 of Jackson *et al.* (2000), COV-OBS of Gillet *et al.* (2013) and CHAOS-4 of Olsen *et al.* (2014). We investigate the possible impact of small scales and we test the numerical significance of the $\dot{E}_b$ values.

Next in Section 4.2, we combine core field and SV models together with core flow models inferred from the geomagnetic SV. We calculate magnetic to magnetic and kinetic to magnetic energy transfer spectra. Both matrices and integrated quantities are analysed.

We use the historical geomagnetic field and SV model gufm1 of Jackson *et al.* (2000) for the period 1840–1990, and the satellites-based model CHAOS-4 (Olsen *et al.* 2014) for the period 1997–2011. To calculate energy transfers we use the purely helical core flow model of Amit & Olson (2006) in conjunction with gufm1 from which it was inverted. The main parameter in this flow model is k, the assumed ratio of tangential divergence to radial vorticity (Amit & Olson 2004). We explore the dependence of our results on flow models obtained with different k values.

4.1 Secular variation of the total geomagnetic energy

We start by calculating the SV of the total geomagnetic energy based on the historical field and SV model gufm1 (Jackson *et al.* 2000). Non-zero values, if robust, imply the existence of core upwelling/downwelling. This interpretation is significant because radial motions just below the CMB may be inferred based on geomagnetic field and SV models only, without relying on either special points (Whaler 1980) or core flow models (e.g. Holme 2015). However, this interpretation is prone to two possible problems. First, small-scale field and SV contributions that are missing in the models might balance $\dot{E}_b$ from the high degrees. Second, the non-zero numerical values might be insignificant.

To check the possibility that $\dot{E}_b$ inferred from the observed high degrees field and SV is balanced by non-observed small scales, we consider low-pass filtered field and SV models. The low-pass filter is defined by

$$F(n) = \begin{cases} 1, & n \leq n_0 \\ \cos\left(\frac{\pi}{2} \frac{n-n_0}{n_{\max}-n_0}\right), & n > n_0 \end{cases} \qquad (31)$$

where n is the spherical harmonic degree, n_0 is the degree from which the filtering starts and $n_{\max}$ is the truncation degree. When $n_0 = n_{\max}$, $F(n)$ is unity for all spherical harmonic degrees, and truncation (rather than filtering) is applied.

In Fig. 1, we present $\dot{E}_b$ (10) as a function of time based on the field and SV model gufm1 (Jackson *et al.* 2000) with $n_{\max} = 8$ (left) and $n_{\max} = 14$ (right). Solid lines correspond to low-pass filters with different n_0 values; Dashed lines correspond to non-filtered field and SV. For both $n_{\max} = 8$ and $n_{\max} = 14$ $\dot{E}_b$ does not vanish when high degrees contributions are added. There is some divergence of the curves towards more recent years due to the increasing amount of data and therefore increasing power of the geomagnetic field and SV models. However, overall there is no tendency of $\dot{E}_b$ towards zero with increasing spatial resolution.

The maps in Fig. 2 represent the integrand of $\dot{E}_b$ for two arbitrary years (1900 and 1980) and for $n_{\max} = 8$ and $n_{\max} = 14$. These maps show clearly that the spatial distribution of sources and sinks of $\dot{E}_b$

is very complex with several regions of opposite sign structures that tend to cancel each other. It therefore requires a careful analysis of the numerical significance of a non-zero integral of this quantity.

Fig. 3 shows the ratio ε_e (24) as a function of time with different low-pass filters. The similarity between the curves in Fig. 3 (which represent the level of cancellation of the sources and sinks of $\dot{E}_b$) and the corresponding curves in Fig. 1 (which is the actual change) suggests that $\dot{E}_b$ is indeed numerically significant.

In Figs 4 and 5, we compare the ratios ε_e (eq. 24) and ε_{mz} (eq. 25) as functions of $n_{\max}$ and of time respectively. In addition to the historical geomagnetic field model gufm1 (Jackson *et al.* 2000), we also calculated these ratios for a family of 100 models from COV-OBS (Gillet *et al.* 2013). In this ensemble of models, data uncertainties are accounted for via a scatter in the values of the field and SV Gauss coefficients, with increasing scatter at larger degrees. This ensemble of models may therefore represent possible small random perturbations to the field.

In Fig. 4, we show both ratios ε_e and ε_{mz} as functions of $n_{\max}$ for three arbitrary years for the gufm1 and COV-OBS models. Both ε_e and ε_{mz} are almost model independent until degree 8. When higher degrees are added, the ratios based on gufm1 and COV-OBS diverge. In addition, including high degrees increases the scatter of ε_e in COV-OBS, but not of ε_{mz}. In 1980 based on gufm1, ε_e and ε_{mz} are comparable for any $n_{\max}$. In the same year based on COV-OBS, the two ratios are comparable for low $n_{\max}$. On approach to $n_{\max} = 14$ the scatter in ε_e includes dominance of either ratio, while the mean values are comparable. In 1940 based on gufm1, ε_e dominates for any $n_{\max}$. In the same year based on COV-OBS, ε_e dominates for low $n_{\max}$. Again at higher truncations, the scatter in ε_e includes dominance of either ratio, while the mean values are comparable. In 1900 the situation is reversed, with overall dominance of ε_{mz} although the scatter in ε_e at high $n_{\max}$ offers some models with dominance of ε_e. Overall, Fig. 4 demonstrates that due to uncertain small scales the geomagnetic data cannot provide definite evidence for non-zero total energy change. However there is an indication for probable comparable ε_e and ε_{mz} values, which would suggest non-zero total energy change. Perhaps more importantly, Fig. 4 shows convergence of ε_e with increasing $n_{\max}$, which may be
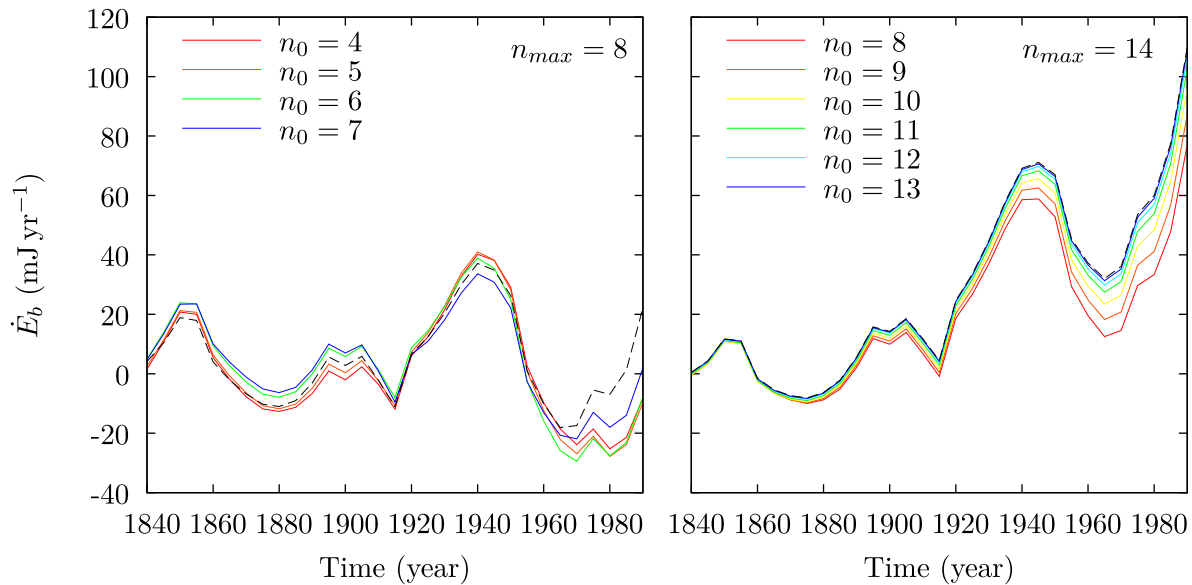
Figure 1. Secular variation of the total geomagnetic energy as a function of time based on the field and SV model gufm1 (Jackson *et al.* 2000) with $n_{\max} = 8$ (left) and $n_{\max} = 14$ (right). Here, $\dot{E}_b$ is expressed in Joule per year. Solid lines represent low-pass filter with different n_0 values; dashed lines denote non-filtered field and SV.
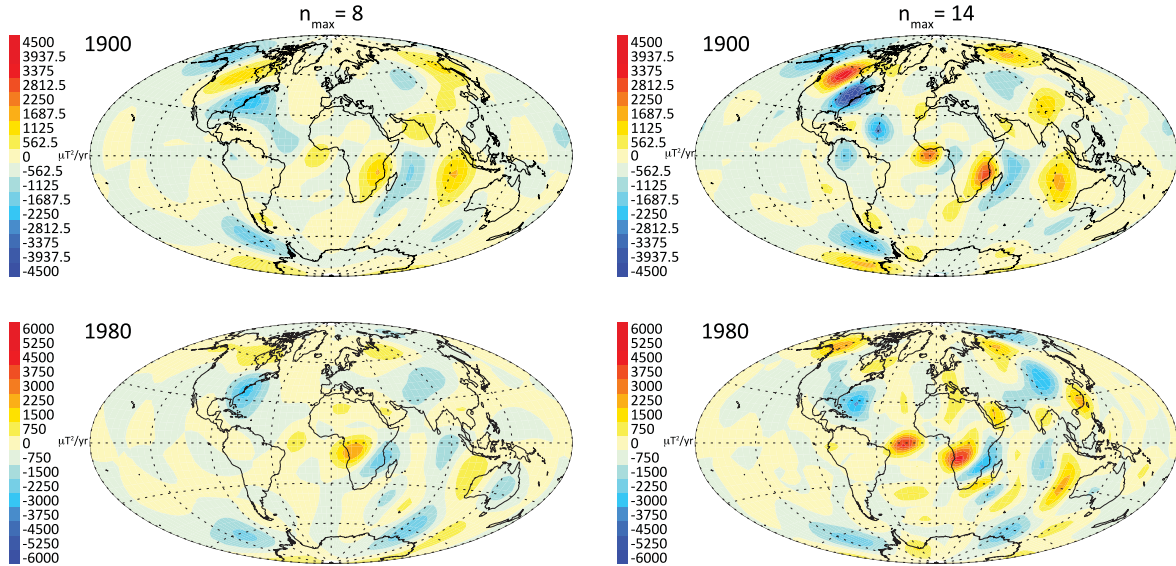
Figure 2. Maps of $B_r \partial B_r/\partial t$ (non-filtered) for the years 1900 (top) and 1980 (bottom). The left column is with $n_{max} = 8$, the right is with $n_{max} = 14$.
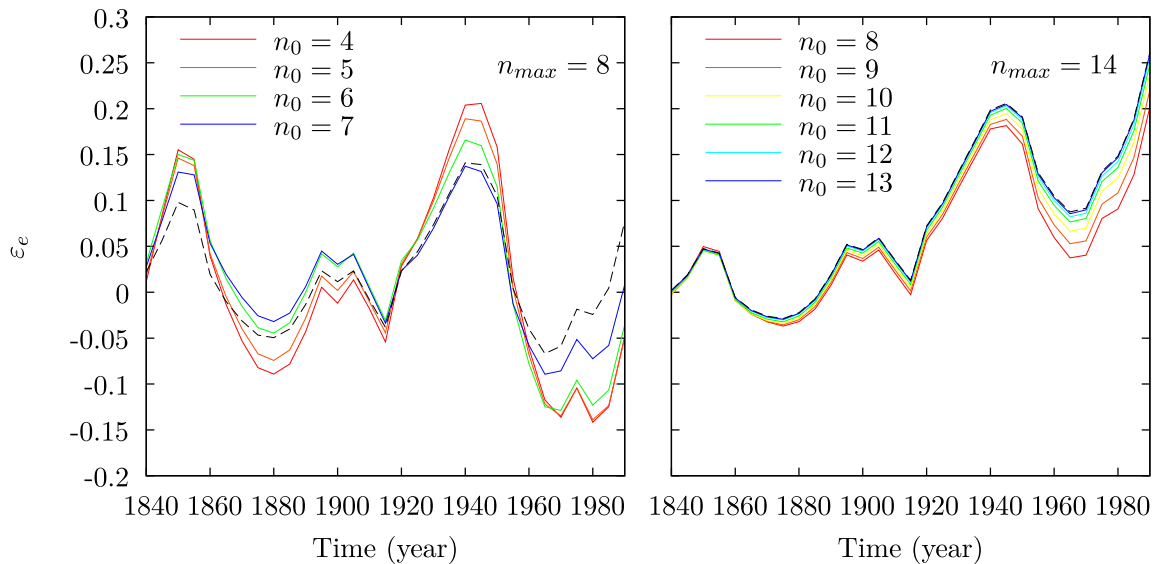
Figure 3. Ratio ε_e (24) as a function of time based on the gufm1 model (Jackson *et al.* 2000) with different low-pass filters. Solid lines denote different n_0 values. Dashed lines represent non-filtered fields. In the left and right plots the field and SV are truncated at $n_{max} = 8$ and $n_{max} = 14$, respectively.

considered as further indication that the total energy change is indeed non-zero.

In Fig. 5 based on gufm1, the two ratios exhibit comparable values (red dotted and solid lines). Interestingly, the two ratios for gufm1 are clearly anti-correlated; Local maxima in ε_e (solid red line) seem to occur at the same time as local minima in ε_{mz} (dotted red line) and vice-versa. Calculation of ε_e excluding the dipole field and SV (green solid curve) result in a rather uniform decrease at all times, hence the anticorrelation persists. A similar anti-correlation also appears for COV-OBS when considering $n_{max} = 8$ (not shown). For all COV-OBS models, ε_e is comparable and in most cases even larger than ε_{mz}. Since the SV of the geomagnetic axial dipole during the historical era is known to be significantly non-zero (e.g. Bloxham & Jackson 1992; Olson & Amit 2006; Finlay 2008), these comparable ratios further testify for the probable numerical significance of $\dot{E}_b$. Note however that the values of ε_e based on gufm1 and COV-OBS are rather different. In COV-OBS at most epochs ε_e is non-zero for the entire ensemble. Using the results of COV-OBS to estimate an

error bar for gufm1, the ε_e value of the latter would include zero within its range.

Finally, we examine $\dot{E}_b$ based on the satellites field and SV model CHAOS-4 (Olsen *et al.* 2014). The maps (Fig. 6) show the integrand of $\dot{E}_b$ for the year 2005. As in Fig. 2, the distribution of sinks and sources is very complex and tends to cancel each other. In Fig. 7, we represent the ratios ε_e and ε_{mz} based on CHAOS-4 as functions of time (top) and of n_{max} (bottom). Again we find that both ratios have the same order of magnitude and the two ratios tend to a non-zero asymptotic value when the high degrees contributions are added.

4.2 Energy transfer spectra

We now combine core field and flow models to calculate magnetic to magnetic $\dot{E}_{bb}$ and kinetic to magnetic $\dot{E}_{ub}$ energy transfers. Fig. 8 compares the SV of total geomagnetic energy (eq. 10, solid line) with that based on a core flow model (Amit & Olson (2006), eqs 15
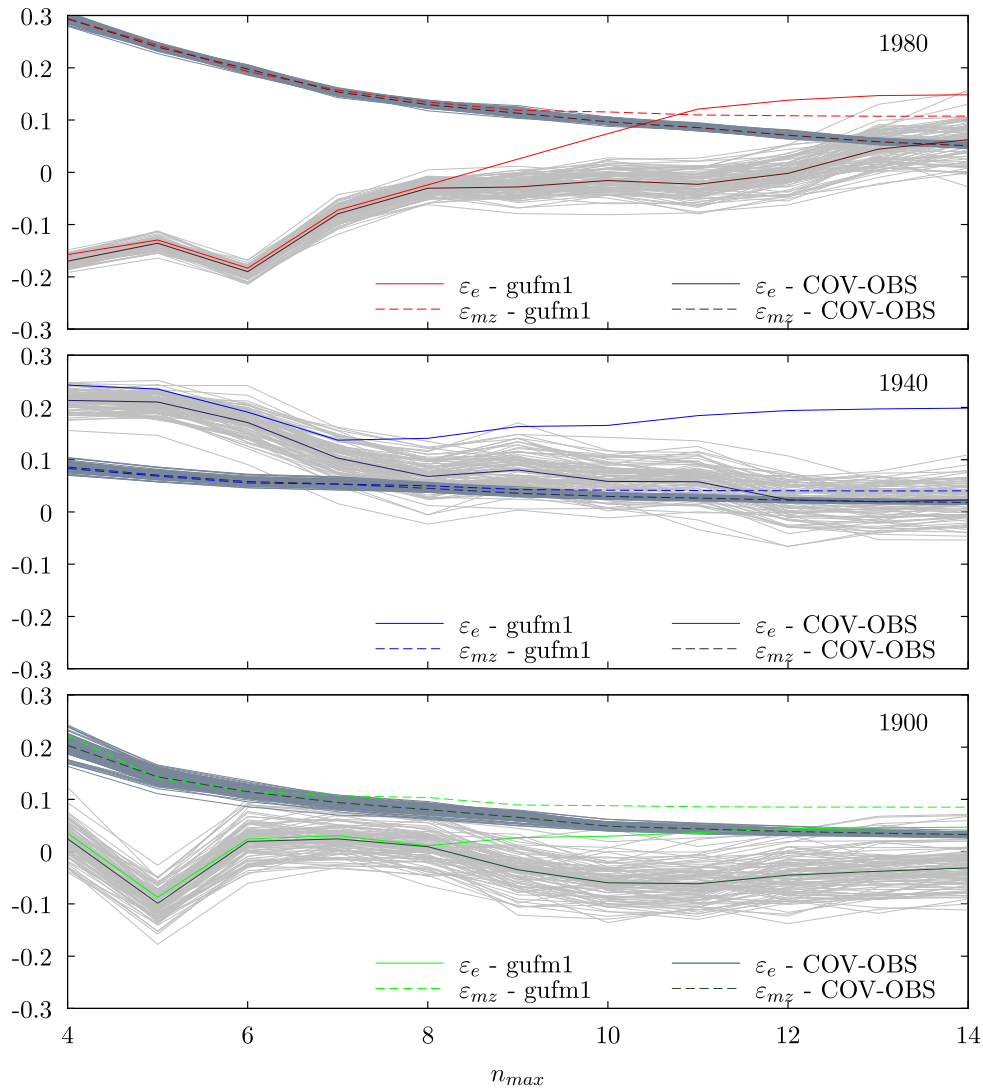
Figure 4. Ratio ε_e (solid lines) and ε_{mz} (dashed lines) as a function of n_{max} (non-filtered) for three arbitrary years (1980, 1940 and 1900), using gufm1 (coloured lines) and the mean of COV-OBS (dark lines). The family of 100 COV-OBS models is presented in light and dark grey solid lines for ε_e and ε_{mz}, respectively.
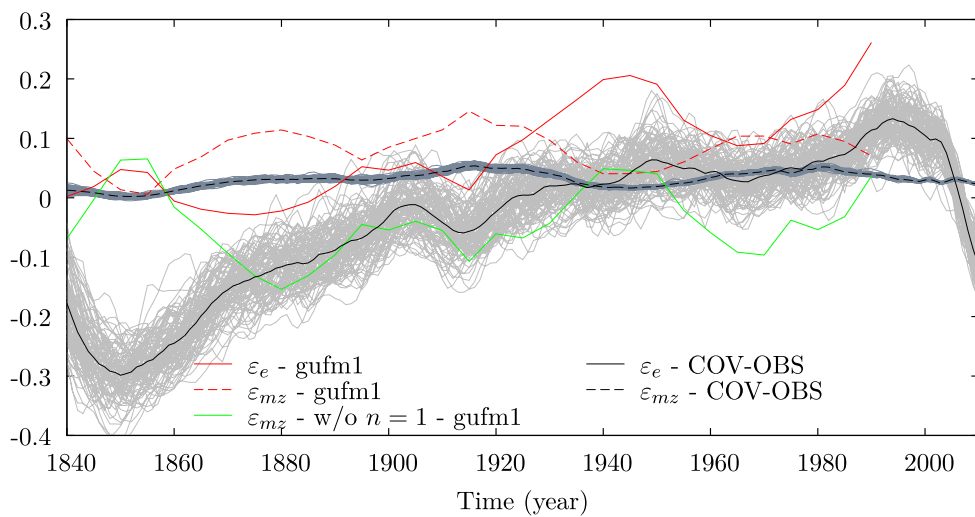
Figure 5. Ratio ε_e (solid line) and ε_{mz} (dashed line) as a function of time (non-filtered), using gufm1 (red lines) and the mean of COV-OBS (dark lines). The family of 100 COV-OBS models is presented in light and dark grey solid lines for ε_e and ε_{mz}, respectively. The green solid line denotes the ratio ε_e excluding the dipole field and SV. The core field and SV models are expanded until spherical harmonic degree 14.
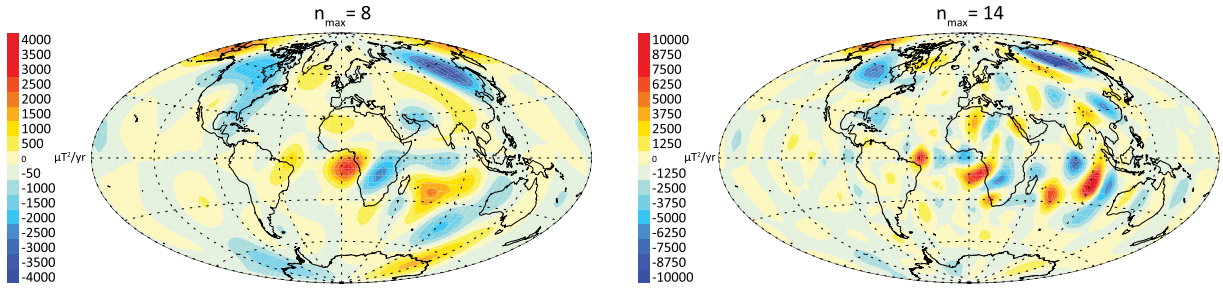
Figure 6. As in Fig. 2 based on the model CHAOS-4 (Olsen *et al.* 2014) for the year 2005. Note the difference between the colour scales of two n_{max} maps.
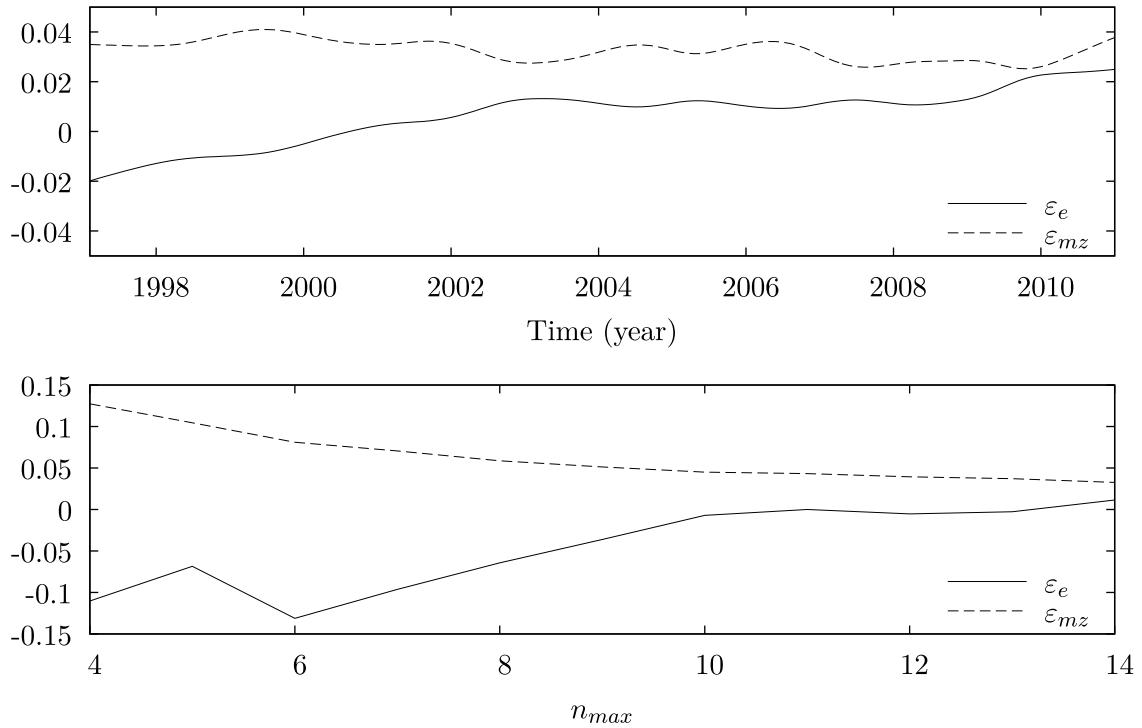

Figure 7. Ratio ε_e (solid line) and ε_{mz} (dashed line) based on the field and SV model CHAOS-4 (Olsen *et al.* 2014) as a function of time (top) for $n_{max} = 14$ and as a function of n_{max} (bottom) for the year 2005.
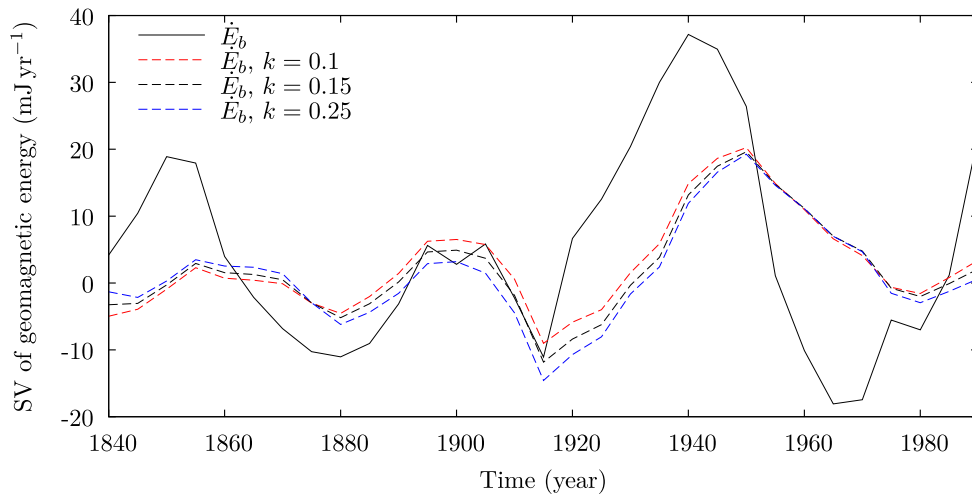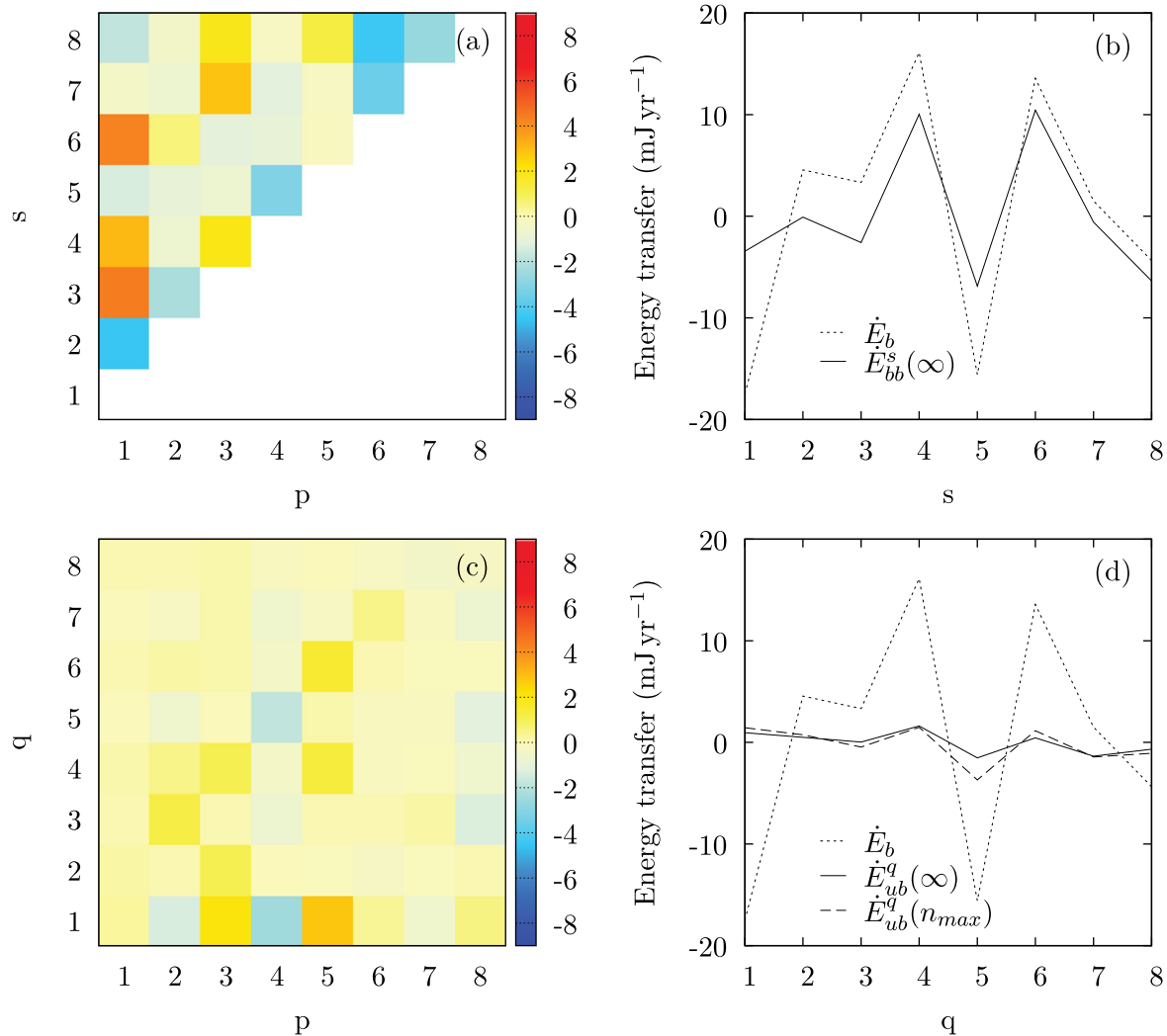

Figure 8. Secular variation of the total geomagnetic energy (solid line) and the total of kinetic to magnetic energy transfer spectrum based on core flow models (dashed lines) with $k = 0.1$ (red), $k = 0.15$ (black) and $k = 0.25$ (blue). The core field and SV model is expanded until spherical harmonic degree 8.

Figure 9. Energy transfer spectra for the time-average of the interval 1840–1910. Magnetic to magnetic (a) and kinetic to magnetic (c) energy transfer matrices $\dot{E}_{bb}(p, s)$ and $\dot{E}_{ub}(p, q)$, respectively. (b,d) The observed energy transfer $\dot{E}_b$ (dotted line), the total energy transfers $\dot{E}_{bb}^s(\infty)$ and $\dot{E}_{ub}^q(\infty)$ (solid black lines) and the kinetic to magnetic energy transfer within the observed spectrum $\dot{E}_{ub}^q(n_{max})$ (dashed line), all in mJ yr^{-1}. In panel (b), the dashed line is practically identical to the solid line.

and 22, dashed lines) for the historical period 1840–1990. Note that the inversion method of Amit & Olson (2006) operates in physical (rather than spectral) space and as such there is no preference to fitting any particular SV coefficient. Despite this naive approach, the two quantities follow similar trends, although some discrepancies appear. For example, the curves are on-phase around 1900 but some phase shift appears at earlier and later periods. The discrepancies are due to imperfections in the core flow model in terms of reproducing the integral of the quantity shown in Fig. 2. This integral quantity is small compared to its integrand, hence it is sensible that the core flow model is not capable of perfectly reproducing it, in analogy to the limited reproducibility of the axial dipole SV by core flow models (Olson & Amit 2006; Finlay *et al.* 2016). The difference between different k values is small (dashed lines in Fig. 8).

In Figs 9–11, we examine the same time-average periods as in Huguet & Amit (2012), this time for both $\dot{E}_{bb}$ as well as $\dot{E}_{ub}$. The three time-average periods correspond to different patterns of alternating minima/maxima in the energy spectrum $\dot{E}_{bb}^s$ (Huguet & Amit 2012). The periods 1840–1910 and 1955–1990 are characterized by even maxima and odd minima and by odd maxima and even

minima, respectively. The period 1915–1950 exhibits relatively smooth pattern of $\dot{E}_{bb}^s$. The matrices $\dot{E}_{bb}(p, s)$ are in agreement with the matrices in figs 9–11 of Huguet & Amit (2012), despite introducing the factor relating the magnetic power and energy (see eq. 19), and despite accounting for $\dot{E}_{ub}(p, q)$. This similarity is mostly because $\dot{E}_{ub}$ which depends on the poloidal flow is smaller than $\dot{E}_{bb}$ which mostly depends on the dominant toroidal flow. In contrast, Huguet & Amit (2012) found some differences between the integrated transfer within the observed spectrum $\dot{E}_{bb}^s(n_{max})$ and the integrated transfer including energy leaking beyond $\dot{E}_{bb}^s(\infty)$. Here we find that these two integrated magnetic to magnetic transfer quantities are practically identical.

In the time-average period 1840–1910, inverse cascade transfers magnetic energy continuously from high to low magnetic field degrees while non-local transfer appears from the dipole to higher degrees (Fig. 9a). In addition, even maxima and odd minima dominate the spectrum of $\dot{E}_{bb}^s(\infty)$ (Fig. 9b). The spectrum $\dot{E}_{bb}^s(n_{max})$ based on the matrix is not shown here because it is practically identical to the solid line in Fig. 9(b), that is, there is very little loss of energy to degrees beyond n_{max}. Fig. 9(c) shows the matrix $\dot{E}_{ub}(p, q)$ representing kinetic to magnetic energy transfer. Note that $\dot{E}_{ub}(p, q)$
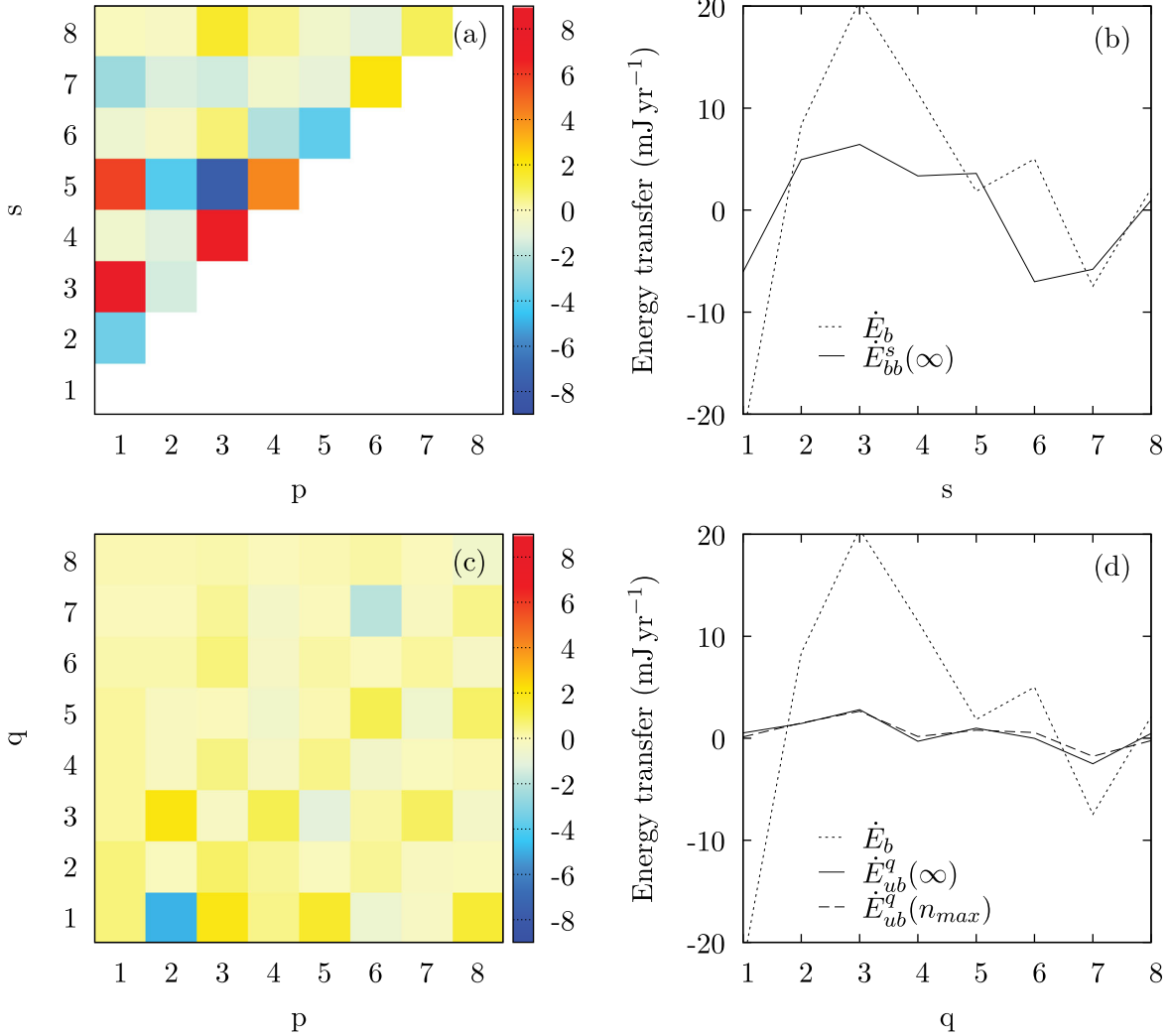
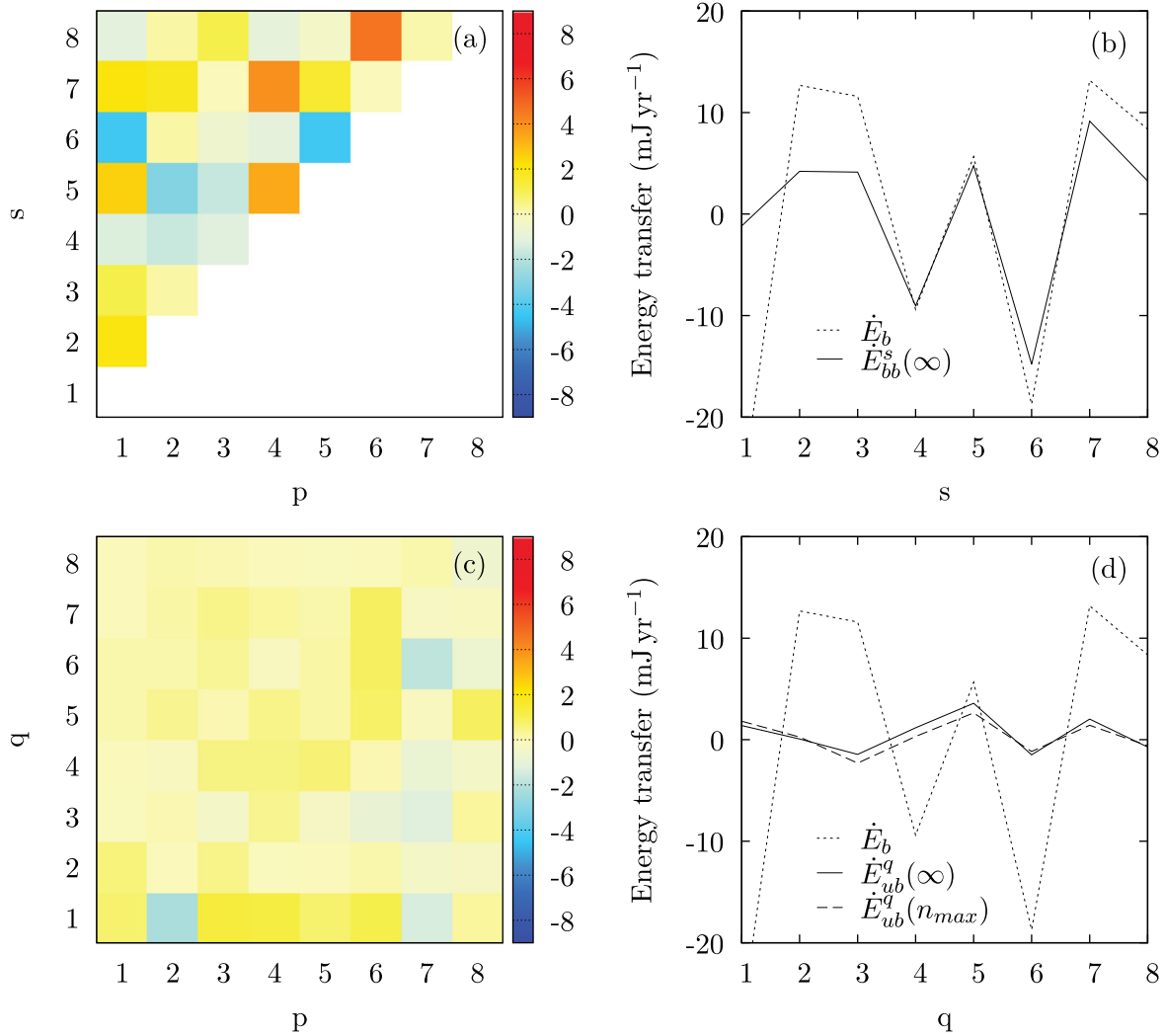**Figure 10.** As in Fig. 9 for the time-average of the interval 1915–1950.

is overall weaker than $\dot{E}_{bb}(p, s)$. The matrix $\dot{E}_{ub}(p, q)$ is concentrated above and below the main the diagonal and on the lowest line, that is, kinetic energy is transferred to neighbouring degrees of the magnetic energy as well as kinetic energy of various degrees are directly injected to the dipole field, respectively. Some magnetic energy is transferred to degree 8 of the flow. The spectrum of $\dot{E}_{ub}^q(\infty)$ and the spectrum of $\dot{E}_{ub}^q(n_{max})$ based on the matrix slightly differ (Fig. 9d) due to some loss of energy to small scales.

Fig. 10 shows the same images for the time-average period 1915–1950. Again, as in Huguet & Amit (2012), both forward magnetic to magnetic energy cascade and non-local transfer from the dipole to higher degrees are observed (Fig. 10a). The pattern of the spectrum $\dot{E}_{bb}^s(\infty)$ is smooth without alternating maxima/minima in the intermediate degrees (Fig. 10b). The matrix $\dot{E}_{ub}(p, q)$ is concentrated in lines 1 and 3, that is, kinetic energy of various degrees are transferred to the dipole and the octupole fields respectively (Fig. 10c). Some magnetic energy is exchanged with degree 6 of the flow which produces the maxima and minima in degrees 6 and 7, respectively.

Finally, in the time-average 1955–1990, the spectrum $\dot{E}_{bb}^s(\infty)$ has reversed to odd maxima and even minima (Fig. 11b). The matrix $\dot{E}_{ub}(p, q)$ is concentrated on degree one of the magnetic field, that is, energy from various degrees of the flow is exchanged with the

dipole. In addition, magnetic energy is transferred to degree 7 of the flow (see negative $\dot{E}_{ub}(p, q)$ in column 7 of Fig. 11c), resulting in the minima in the integrated kinetic to magnetic transfer in degrees 3 and 6 (Fig. 11d).

Finally, we calculate the matrices $\dot{E}_{bb}(p, s)$ and $\dot{E}_{ub}(p, q)$ with the satellites-based model CHAOS-4 (Olsen *et al.* 2014) for the year 2005. The CHAOS-4 model allows considering higher resolution features, so we use $n_{max} = 12$ instead of $n_{max} = 8$ for gufm1. In Fig. 12(a), the matrix $\dot{E}_{bb}(p, s)$ shows a complex pattern with all degrees participating in the magnetic to magnetic transfer. Note however that the most significant magnetic to magnetic transfers cluster around the main diagonal, corresponding to local (or almost local) energy transfer. The spectrum $\dot{E}_{bb}^s(\infty)$ (Fig. 12b) has an alternating pattern: odd maxima and even minima between degrees 3 and 7 and even maxima and odd minima between degrees 8 and 12. Lines 4 and 6 are mainly negative and columns 4 and 6 are mainly positive, reflecting the minima in the integrated spectrum for these degrees. In Fig. 12(c), the matrix $\dot{E}_{ub}(p, q)$ is mostly concentrated near the main diagonal, at line 1 (i.e. energy exchange between various degrees of the flow and the dipole field) and column 12 (i.e. energy exchange between various degrees of the field and degree 12 of the flow). As in the analysis of gufm1 (Figs 9–11), the integrated kinetic to magnetic transfer (Fig. 12d) is smaller than the integrated

Figure 11. As in Fig. 9 for the time-average of the interval 1955–1990.

magnetic to magnetic transfer (Fig. 12b). The strongest $\dot{E}_{ub}(p, q)$ is in 8 to 1, that is, kinetic energy of flow degree 8 is transferred to the dipole field. In column 8, there are two positive transfers (8 to 7, 8 to 12) which produce maxima in 7 and 12 in Fig. 12(d). The minimum in 6 in Fig. 12(d) is due to negative 5 to 6. Degree 12 of the flow transfers energy to the dipole and to degree 11 of the field thus resulting in maxima between degree 12 of the flow and the integrated spectrum for those degrees, whereas opposite in degrees 2, 3 and 9 of the field cause minima in the integrated spectrum at the latter degrees.

5 DISCUSSION

We revisited the theory for magnetic to magnetic and kinetic to magnetic energy transfers in 3-D with full magnetic field vector (Alexakis *et al.* 2005a; Debliquy *et al.* 2005; Mininni *et al.* 2005; Carati *et al.* 2007). We applied this theory to the 2-D case with radial magnetic field only. In the 3-D case, the magnetic to magnetic energy transfer is fully controlled by the advection term (eq. 6), whereas in the 2-D case $\dot{e}_{bb}$ is due to the advection term plus half the stretching term (eq. 14). Therefore, the kinetic to magnetic energy transfer is due to the stretching term in the 3-D case

(eq. 7), whereas $\dot{e}_{ub}$ is due to half the stretching term in the 2-D case (eq. 15).

Because the spectrum of kinetic to magnetic energy transfer depends on the stretching term only, and because the total magnetic to magnetic energy transfer is identically zero, non-zero SV of the total magnetic energy is suggestive of the existence of upwelling/downwelling at the top of the Earth's core. We tested the robustness of non-zero $\dot{E}_b$ values in terms of unknown small scales and numerical significance. Applying a low-pass filter on the field and SV models, we demonstrated that adding small scales does not tend to diminish $\dot{E}_b$ (Fig. 1). These results suggest that the non-zero values of the SV of the total geomagnetic energy may not necessarily be an artefact of unknown small scales.

To assess the numerical significance of non-zero $\dot{E}_b$ values, we analysed maps of $\dot{E}_b$ sources and sinks. These maps show complex patterns with several regions of opposite sign contributions which tend to cancel each other (Figs 2 and 6). To quantify the level of cancellation of the $\dot{E}_b$ sources and sinks, we calculated the ratio ε_e (eq. 24). A similar integral ratio has recently been used to calculate the level of cancellations of advective contributions to axial dipole SV (Finlay *et al.* 2016). The similar temporal trends of ε_e and $\dot{E}_b$ provides a first indication that the non-zero value of $\dot{E}_b$ is numerically significant (Fig. 3). Comparing ε_e with the level of cancellation
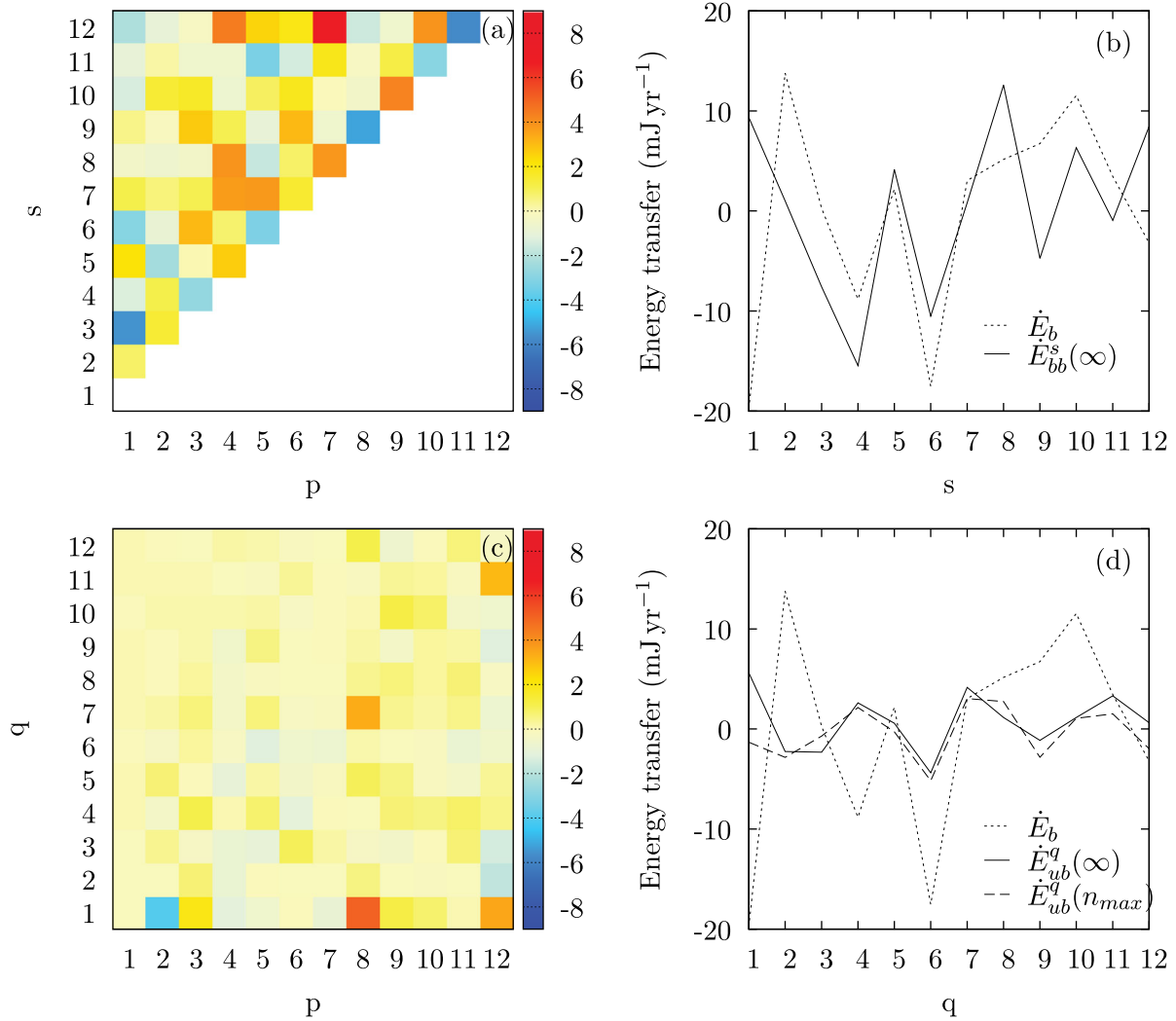
Figure 12. As in Fig. 9 for the year 2005 for the model CHAOS-4 (Olsen *et al.* 2014).

of axial dipole sources and sinks ε_{mz} gives same order of magnitude (Figs 4, 5 and 7). A detailed error analysis using 100 models from the ensemble of Gillet *et al.* (2013) reveals that at high degrees both ratios may dominate, rendering the significance of the non-zero total energy change inconclusive. However, in Figs 4 and 5 both the gufm1 values and the mean COV-OBS values indicate comparable ε_e and ε_{mz}, with a scatter of ε_e around its mean value. These results indicate significant likelihood that the two ratios are indeed comparable. Because the SV of the geomagnetic axial dipole is known to be significantly non-zero (e.g. Bloxham & Jackson 1992; Olson & Amit 2006; Finlay 2008), the similar magnitudes of ε_e and ε_{mz} provides a second indication for the numerical significance of $\dot{E}_b$. Note that for gufm1 the two ratios are clearly anti-correlated. A peak in ε_{mz} coincides with a minimum in ε_e and corresponds to a steeper decrease of geomagnetic axial dipole and to a lower decrease or increase of total geomagnetic field energy. This suggests that a large fraction of the dipole energy is transferred to large scales within the observed spectrum.

These results suggest the presence of upwelling/downwelling at top of Earth's core. Several studies inferred radial motions at the top of the core based on analysis of geomagnetic SV, for example upwelling below the north polar cap (Olson & Aurnou 1999; Chulliat *et al.* 2010), downwelling below the Indian Ocean (Amit &

Pais 2013; Amit 2014), magnetic flux expulsion below equatorial Atlantic (Chulliat & Olsen 2010) and the general need for poloidal flow to better explain the global geomagnetic SV (Whaler 1986; Beggan & Whaler 2008). In contrast, seismic studies and mineral physics calculations support stable layer at the top of the Earth's core due to either thermal (Gubbins *et al.* 1982; Labrosse *et al.* 1997; Lister & Buffett 1998) or compositional stratification (Helffrich & Kaneshima 2010; Pozzo *et al.* 2012; Gubbins & Davies 2013; Davies *et al.* 2015). There are scenarios that may reconcile stable stratification with poloidal flow at the top of the core. The fluid below the stable layer may penetrate it (Buffett & Seagle 2010). Lower mantle thermal heterogeneity suggested by observed seismic anomalies may drive thermal winds that can stir the upper outer core (Sreenivasan 2009; Aurnou & Aubert 2011). The effectiveness of such scenarios depends on the depth of the stratified layer. The presence of upwelling/downwelling that we inferred from the SV of the total geomagnetic energy may indicate whole outer core convection (e.g. Whaler 1986). Alternatively, MAC waves may accommodate radial motions through a stratified layer (Buffett 2014; Buffett *et al.* 2016). However, the radial motions associated with these waves are very large-scale and balanced in latitude (Buffett 2014; Buffett *et al.* 2016), in contrast to tangential geostrophic core flow models that exhibit smaller scales and equatorial concentration of

tangential divergence and subsequent magnetic field stretching (see e.g. fig. 3d of Amit & Pais 2013). Since Buffett (2014) and Buffett *et al.* (2016) derived his waves solution based on the tangential geostrophic core flow model of Jackson (1997), the patterns of radial motions of the core flow model and the fitted MAC waves are probably inconsistent.

Next, we combined core field and flow models to calculate the detailed transfer matrices. Comparison of $\dot{E}_b$ with the corresponding value based on a core flow model (Amit & Olson 2006) shows similar trends, with the difference being due to the core flow model imperfections. The matrices $\dot{E}_{bb}(p, s)$ are very similar to those of Huguet & Amit (2012), despite the fact that the earlier paper ignored $\dot{E}_{ub}(p, q)$, because the core flow model is dominantly toroidal. These matrices show a very complex behaviour with both local and non-local energy transfers (Figs 9a–12a). The spectra of $\dot{E}_{bb}^s$ show alternating maxima and minima (Figs 9b–12b).

The matrices of $\dot{E}_{ub}(p, q)$ are much weaker than those of $\dot{E}_{bb}(p, s)$, again because poloidal flow is smaller than the toroidal flow at the CMB. The main $\dot{E}_{ub}(p, q)$ contributions are concentrated on degree one of the magnetic field and just above and below the main diagonal of the matrix (Figs 9c–12c). The same patterns are observed in self-consistent 3-D MHD numerical simulations (Alexakis *et al.* 2005b; Mininni *et al.* 2005; Alexakis *et al.* 2007).

Analysis of CHAOS-4 (Fig. 12) gives a glimpse to the energy transfers associated with higher degrees. In CHAOS-4 we found that the magnetic to magnetic energy transfer is more local than in gufm1. As in gufm1, the CHAOS-4 spectrum of $\dot{E}_{bb}^s$ is characterized by alternating minima/maxima. Furthermore, as in gufm1 the matrix $\dot{E}_{ub}(p, q)$ in CHAOS-4 is concentrated around the main diagonal and from the dipole to different flow degrees, but in addition the highest degree of the flow (invisible with gufm1) is involved in significant energy exchanges with various degrees of the field.

The spectra of $\dot{E}_{bb}^s$ are in general agreement with those of $\dot{E}_b$ in terms of sign and magnitude except for the dipole (Figs 9b–12b). Because the dipole SV is smaller than the SV of higher degrees, the core flow recovers dipole SV less well than higher harmonics SV (Jackson 1997; Whaler & Davis 1997). Nevertheless, dipole SV temporal trend is reasonably captured by our flow model (Olson & Amit 2006; Amit & Olson 2008). The SV of the magnetic energy (per degree) corresponds to the SV weighted by the field, so the strong dipole field amplifies the error in the recovery of the dipole SV by the flow. In addition, the axial dipole field depends only on latitude, so zonal flows that are thought to be dominant in the core (e.g. Olson & Aurnou 1999; Hulot *et al.* 2002; Amit & Olson 2006; Holme & Olsen 2006; Amit & Pais 2013; Aubert *et al.* 2013) produce identically zero axial dipole SV. As a result, magnetic diffusion (which is not accounted for in most core flow models) contaminates dipole SV much more than it contaminates other harmonics (Holme & Olsen 2006).

Our formalism to calculate magnetic to magnetic and kinetic to magnetic energy transfers requires knowledge of the radial magnetic field and its SV on the CMB together with knowledge of the flow at the top of the core that induced the SV. A first application of this formalism involves the field and its SV (without the flow): The SV of the total field, if non-zero, provides a proof for the existence of upwelling/downwelling at the top of the core or for the waves in a stratified layer at the top of the core (Buffett 2014; Buffett *et al.* 2016). A second application involves a core flow model to yield the detailed matrices of magnetic to magnetic and kinetic to magnetic energy transfers. Clearly the results of these applications rely on the robustness of the time-dependent geomagnetic field and core flow model, both of which are uncertain. In particular, core flow models

suffer from various inherent problems (e.g. Holme 2015). For our purposes, the resulting poloidal flow which is responsible for the kinetic to magnetic energy transfer is strongly dependent on the physical assumption applied in the geomagnetic SV inversion. Here we merely demonstrate the applicability of our formalism using a specific core flow model, therefore extra caution is required in the interpretation of the results. Applying our formalism using other field models (e.g. Sabaka *et al.* 2002; Finlay *et al.* 2012; Gillet *et al.* 2013), and in particular using other core flow models that rely on different physical assumptions and numerical techniques (e.g. Holme & Olsen 2006; Gillet *et al.* 2009; Asari & Lesur 2011; Amit & Pais 2013; Aubert *et al.* 2013), may validate or contradict our results. Overall, unraveling the transfer of geomagnetic energy to different field and flow degrees will shed light on the convective state of the upper outer core and the dynamical origin of the dipole decrease.

REFERENCES

Alexakis, A., Mininni, P. & Pouquet, A., 2005a. Imprint of large-scale flows on turbulence, *Phys. Rev. Lett.,* **93,** 264503, doi:10.1103/PhysRevLett.95.264503.

Alexakis, A., Mininni, P. & Pouquet, A., 2005b. Shell to shell energy transfer in MHD. I. Steady state turbulence, *Phys. Rev. E.,* **72,** 046301, doi:10.1103/PhysRevE.72.046301.

Alexakis, A., Mininni, P. & Pouquet, A., 2007. Turbulent cascades, transfer, and scale interactions in magnetohydrodynamics, *New J. Phys.,* **9,** 1–20.

Amit, H., 2014. Can downwelling at the top of the Earth's core be detected in the geomagnetic secular variation?, *Phys. Earth planet. Inter.,* **229,** 110–121.

Amit, H. & Olson, P., 2004. Helical core flow from geomagnetic secular variation, *Phys. Earth planet. Inter.,* **147,** 1–25.

Amit, H. & Olson, P., 2006. Time-average and time-dependent parts of core flow, *Phys. Earth planet. Inter.,* **155,** 120–139.

Amit, H. & Olson, P., 2008. Geomagnetic dipole tilt changes induced by core flow, *Phys. Earth planet. Inter.,* **166,** 226–238.

Amit, H. & Olson, P., 2010. A Dynamo Cascade Interpretation of the Geomagnetic Dipole Decrease, *Geophys. J. Int.,* **181,** 1411–1427.

Amit, H. & Pais, M.A., 2013. Differences between tangential geostrophy and columnar flow, *Geophys. J. Int.,* **194**(1), 145–157.

Asari, S. & Lesur, V., 2011. Radial vorticity constraint in core flow modeling, *J. geophys. Res.,* **116**(B11), doi:10.1029/2011JB008267.

Aubert, J., Aurnou, J. & Wicht, J., 2008. The magnetic structure of convection-driven numerical dynamos, *Geophys. J. Int.,* **172,** 945–956.

Aubert, J., Finlay, C.C. & Fournier, A., 2013. Bottom-up control of geomagnetic secular variation by the Earth's inner core, *Nature,* **502,** 219–223.

Aurnou, J.M. & Aubert, J., 2011. End-member models of boundary-modulated convective dynamos, *Phys. Earth planet. Inter.,* **187**(3), 353–363.

Batchelor, G., 1953. *The Theory of Homogeneous Turbulence,* Cambridge Univ. Press.

Beggan, C. & Whaler, K. Apr. 2008. Core flow modelling assumptions, *Phys. Earth planet. Inter.,* **167,** 217–222.

Bloxham, J. & Jackson, A., 1992. Time-dependent mapping of the magnetic field at the core-mantle boundary, *J. geophys. Res.,* **97,** 19 537–19 563.

Buffett, B., 2014. Geomagnetic fluctuations reveal stable stratification at the top of the Earth's core, *Nature,* **507**(7493), 484–487.

Buffett, B., Knezek, N. & Holme, R., 2016. Evidence for MAC waves at the top of Earth's core and implications for variations in length of day, *Geophys. J. Int.,* **204**(3), 1789–1800.

Buffett, B.A. & Seagle, C.T., 2010. Stratification of the top of the core due to chemical interactions with the mantle, *J. geophys. Res.,* **115**(B4), doi:10.1029/2009JB006751.

Cain, J., Wang, Z., Schmitz, D. & Meyer, J., 1989. The geomagnetic spectrum for 1989 and core-crustal separation, *Geophys. J. Int.,* **97,** 443–447.

Carati, D., Debliquy, O., Knaepen, B., Teaca, B. & Verma, M., 2007. Energy fluxes and shell-to-shell transfers in MHD turbulence, in *Complex Effects in Large Eddy Simulations,* Vol. 56 of Lecture Notes in Computational Science and Engineering, pp. 401–412, eds Kassinos, S., Langer, C., Iaccarino, G. & Moin, P., Springer.

Christensen, U., Wardinski, I. & Lesur, V., 2012. Timescales of geomagnetic secular acceleration in satellite field models and geodynamo models, *Geophys. J. Int.,* **190**(1), 243–254.

Chulliat, A. & Olsen, N., 2010. Observation of magnetic diffusion in the Earth's outer core from Magsat, Ørsted & CHAMP data, *J. geophys. Res.,* **115**(B5), doi:10.1029/2009JB006994.

Chulliat, A., Hulot, G. & Newitt, L., 2010. Magnetic flux expulsion from the core as a possible cause of the unusually large acceleration of the north magnetic pole during the 1990s, *J. geophys. Res.,* **115**(B7), doi:10.1029/2009JB007143.

Currie, R.G., 1973. Geomagnetic line spectra-2 to 70 years, *Astrophys. Space Sci.,* **21**(2), 425–438.

Davidson, P., 2001. *An Introduction to Magnetohydrodynamics,* Cambridge Univ. Press.

Davies, C., Pozzo, M., Gubbins, D. & Alfè, D., 2015. Constraints from material properties on the dynamics and evolution of Earth's core, *Nat. Geosci.,* **8,** 678–685.

Debliquy, O., Verma, M.K. & Carati, D., 2005. Energy fluxes and shell-to-shell transfers in three-dimensional decaying magnetohydrodynamic turbulence, *Phys. Plasmas,* **12**(4), 042309, doi:10.1063/1.1867996.

Finlay, C., 2008. Historical variation of the geomagnetic axial dipole, *Phys. Earth planet. Inter.,* **170,** 1–14.

Finlay, C., Jackson, A., Gillet, N. & Olsen, N., 2012. Core surface magnetic field evolution 2000–2010, *Geophys. J. Int.,* **189**(2), 761–781.

Finlay, C.C., Aubert, J. & Gillet, N., 2016. Gyre-driven decay of the Earth's magnetic dipole, *Nat. Commun.,* **7,** doi:10.1038/ncomms10422.

Frisch, U., 1995. *Turbulence: The Legacy of A.N. Kolmogorov,* Cambridge Univ. Press.

Gillet, N., Pais, M. & Jault, D., 2009. Ensemble inversion of time-dependent core flow models, *Geochem. Geophys. Geosyst.,* **10,** Q06004, doi:10.1029/2008GC002290.

Gillet, N., Jault, D., Finlay, C. & Olsen, N., 2013. Stochastic modeling of the Earth's magnetic field: inversion for covariances over the observatory era, *Geochem. Geophys. Geosyst.,* **14**(4), 766–786.

Gomi, H., Ohta, K., Hirose, K., Labrosse, S., Caracas, R., Verstraete, M.J. & Hernlund, J.W., 2013. The high conductivity of iron and thermal evolution of the Earth's core, *Phys. Earth planet. Inter.,* **224,** 88–103.

Gross, R.S., 2001. A combined length-of-day series spanning 1832–1997: LUNAR97, *Phys. Earth planet. Inter.,* **123**(1), 65–76.

Gubbins, D., 1987. Mechanism for geomagnetic polarity reversals, *Nature,* **326,** 167–169.

Gubbins, D. & Davies, C., 2013. The stratified layer at the core–mantle boundary caused by barodiffusion of oxygen, sulphur and silicon, *Phys. Earth planet. Inter.,* **215,** 21–28.

Gubbins, D., Thomson, C. & Whaler, K., 1982. Stable regions in the Earth's liquid core, *Geophys. J. Int.,* **68**(1), 241–251.

Helffrich, G. & Kaneshima, S., 2010. Outer-core compositional stratification from observed core wave speed profiles, *Nature,* **468**(7325), 807–810.

Holme, R., 2015. Large-Scale Flow in the Core, in *Treatise on Geophysics*, 2nd edn, ed. Schubert, G., pp. 91–113, Elsevier, Oxford.

Holme, R. & De Viron, O., 2013. Characterization and implications of intradecadal variations in length of day, *Nature,* **499**(7457), 202–204.

Holme, R. & Olsen, N., 2006. Core surface flow modelling from high-resolution secular variation, *Geophys. J. Int.,* **166,** 518–528.

Holme, R., Olsen, N. & Bairstow, F., 2011. Mapping geomagnetic secular variation at the core-mantle boundary, *Geophys. J. Int.,* **186,** 521–528.

Huguet, L. & Amit, H., 2012. Magnetic energy transfer at the top of the Earth's core, *Geophys. J. Int.,* **190**(2), 856–870.

Hulot, G., Eymin, C., Langlais, B., Mandea, M. & Olsen, N., 2002. Small-scale structure of the geodynamo inferred from Oersted and Magsat satellite data, *Nature,* **416,** 620–623.

Jackson, A., 1997. Time-dependency of tangentially geostrophic core surface motions, *Phys. Earth planet. Inter.,* **103,** 293–311.

Jackson, L. & Mound, J., 2010. Geomagnetic variation on decadal time scales: What can we learn from Empirical Mode Decomposition?, *Geophys. Res. Lett.,* **37**(14), doi:10.1029/2010GL043455.

Jackson, A., Jonkers, A. & Walker, M., 2000. Four centuries of geomagnetic secular variation from historical records, *Phil. Trans. R. Soc. Lond., A,* **358,** 957–990.

Kolmogorov, A., 1941. The local structure of turbulence in incompressible viscous fluid for very large Reynolds Numbers, *Dokl. Akad. Nauk SSSR,* **30,** 299–303.

Konôpková, Z., McWilliams, R.S., Gómez-Pérez, N. & Goncharov, A.F., 2016. Direct measurement of thermal conductivity in solid iron at planetary core conditions, *Nature,* **534**(7605), 99–101.

Labrosse, S., Poirier, J.-P. & Le Mouël, J.-L., 1997. On cooling of the Earth's core, *Phys. Earth planet. Inter.,* **99**(1), 1–17.

Lessinnes, T., Carati, D. & Verma, M.K., 2009. Energy transfers in shell models for magnetohydrodynamics turbulence, *Phys. Rev. E,* **79**(6), 066307, doi:10.1103/PhysRevE.79.066307.

Lesur, V., Whaler, K. & Wardinski, I., 2015. Are geomagnetic data consistent with stably stratified flow at the core-mantle boundary?, *Geophys. J. Int.,* **201**(2), 929–946.

Lhuillier, F., Fournier, A., Hulot, G. & Aubert, J., 2011. The geomagnetic secular-variation timescale in observations and numerical dynamo models, *Geophys. Res. Lett.,* **38**(9), L09306, doi:10.1029/2011GL047356.

Lister, J.R. & Buffett, B.A., 1998. Stratification of the outer core at the core-mantle boundary, *Phys. Earth planet. Inter.,* **105**(1), 5–19.

Lowes, F., 1974. Spatial power spectrum of the main geomagnetic field, *Geophys. J. R. astr. Soc.,* **36,** 717–730.

Mininni, P., Alexakis, A. & Pouquet, A., 2005. Shell-to-shell energy transfer in magnetohydrodynamics. II. Kinematic dynamo, *Phys. Rev. E,* **72**(4), 046302, doi:10.1103/PhysRevE.72.046302.

Mininni, P.D., 2011. Scale interactions in magnetohydrodynamic turbulence, *Annu. Rev. Fluid Mech.,* **43,** 377–397.

Moffatt, H., 1978. *Magnetic Field Generation in Electrically Conducting Fluids,* Cambridge Univ. Press.

Ohta, K., Kuwayama, Y., Hirose, K., Shimizu, K. & Ohishi, Y., 2016. Experimental determination of the electrical resistivity of iron at Earth's core conditions, *Nature,* **534**(7605), 95–98.

Olsen, N. & Mandea, M., 2008. Rapidly changing flows in the Earth's core, *Nat. Geosci.,* **1,** 390–394.

Olsen, N., Lühr, H., Finlay, C., Sabaka, T., Michaelis, I., Rauberg, J. & Toffner-Clausen, L., 2014. The CHAOS-4 geomagnetic field model, *Geophys. J. Int.,* **197**(2), 815–827.

Olson, P. & Amit, H., 2006. Changes in Earth's dipole, *Naturwissenschaften,* **93,** 519–542.

Olson, P. & Aurnou, J., 1999. A polar vortex in the Earth's core, *Nature,* **402,** 170–173.

Olson, P., Driscoll, P. & Amit, H., 2009. Dipole collapse and reversal precursors in a numerical dynamo, *Phys. Earth planet. Inter.,* **173,** 121–140.

Pais, M. & Jault, D., 2008. Quasi-geostrophic flows responsible for the secular variation of the Earth's magnetic field, *Geophys. J. Int.,* **173**(2), 421–443.

Pozzo, M., Davies, C., Gubbins, D. & Alfè, D., 2012. Thermal and electrical conductivity of iron at Earth's core conditions, *Nature,* **485**(7398), 355–358.

Roberts, P., Yu, Z. & Russell, C., 2007. On the 60-year signal from the core, *Geophys. Astrophys. Fluid Dyn.,* **101**(1), 11–35.

Sabaka, T.J., Olsen, N. & Langel, R.A., 2002. A comprehensive model of the quiet-time, near-Earth magnetic field: phase 3, *Geophys. J. Int.,* **151**(1), 32–68.

Sreenivasan, B., 2009. On dynamo action produced by boundary thermal coupling, *Phys. Earth planet. Inter.,* **177**(3), 130–138.

Takahashi, F., Matsushima, M. & Honkura, Y., 2007. A numerical study on magnetic polarity transition in an MHD dynamo model, *Earth Planets Space,* **59**, 665–673.

Takehiro, S.-I. & Lister, J.R., 2001. Penetration of columnar convection into an outer stably stratified layer in rapidly rotating spherical fluid shells, *Earth planet. Sci. Lett.,* **187**(3), 357–366.

Vidal, J. & Schaeffer, N., 2015. Quasi-geostrophic modes in the Earth's fluid core with an outer stably stratified layer, *Geophys. J. Int.,* **202**(3), 2182–2193.

Vlček, V., de Koker, N. & Steinle-Neumann, G., 2012. Electrical and thermal conductivity of Al liquid at high pressures and tempera-

tures from *ab initio* computations, *Phys. Rev. B,* **85**(18), 184201, doi:10.1103/PhysRevB.85.184201.

Whaler, K., 1980. Does the whole of Earth's core convect?, *Nature,* **287**, 528–530.

Whaler, K., 1986. Geomagnetic evidence for fluid upwelling at the core-mantle boundary, *Geophys. J. R. astr. Soc.,* **86**, 563–588.

Whaler, K. & Davis, R., 1997. Probing the Earth's core with geomagnetism, in *Earth's Deep Interior,* pp. 115–166, ed. Crossley, D., Gordon and Breach.

Whaler, K. & Holme, R., 2007. Consistency between the flow at the top of the core and the frozen-flux approximation, *Earth Planets Space,* **59**, 1219–1229.

Wicht, J. & Olson, P., 2004. A Detailed study of the polarity reversal mechanism in a numerical dynamo model, *Geochem. Geophys. Geosyst.,* **5**, doi:10.1029/2003GC000602.